Commun. Comput. Phys.
doi: 10.4208/cicp.431011.260112s

Vol. **13**, No. 3, pp. 706-724
March 2013

Effects of Inertia and Viscosity on Single Droplet Deformation in Confined Shear Flow

Samaneh Farokhirad[1], Taehun Lee[1,*] and Jeffrey F. Morris[2]

[1] *Department of Mechanical Engineering, City College of City University of New York, New York, New York 10031, USA.*
[2] *Department of Chemical Engineering and Levich Institute, City College of City University of New York, New York, New York 10031, USA.*

Received 31 October 2011; Accepted (in revised version) 26 January 2012

Available online 29 August 2012

Abstract. Lattice Boltzmann simulations based on the Cahn-Hilliard diffuse interface approach are performed for droplet dynamics in viscous fluid under shear flow, where the degree of confinement between two parallel walls can play an important role. The effects of viscosity ratio, capillary number, Reynolds number, and confinement ratio on droplet deformation and break-up in moderately and highly confined shear flows are investigated.

PACS: 47.11.-j, 47.65.Cb

Key words: Lattice Boltzmann method, droplet deformation, confinement.

1 Introduction

The problem of deformation and break-up of an immiscible droplet in shear flows has been studied extensively since the original experiments by Taylor [1]. This problem is of great interest in many science and engineering applications such as emulsification processes, e.g., food industry, polymer blending and oil recovery, and in deformation of biological cells [2]. In these processes two immiscible fluids are mixed to obtain a distribution of droplets of one of the liquids in the other. Therefore, many investigations have been carried out from experimental, numerical, and theoretical points of view, and have shown that droplet deformation in shear flows are governed by four dimensionless parameters, namely, the capillary number (Ca) based on matrix fluid, the Reynolds number (Re) based on the matrix fluid, the viscosity ratio of the droplet viscosity to that of matrix fluid (η) [3], and the confinement ratio defined as the ratio of droplet diameter to the wall separation.

*Corresponding author. *Email addresses:* farokhirad@gmail.com (S. Farokhirad), thlee@ccny.cuny.edu (T. Lee), jmorris@che.engr.ccny.cuny.edu (J. F. Morris)

Megias-Alguacil *et al.* [4] performed an experimental study of droplet deformation under simple shear flow. They used the boundary integral method (BIM) as a numerical tool for validation of the experiment and for measurement of droplet deformation for a wide range of viscosity ratios. Several different values of the capillary number were considered for each η under different experimental conditions. The results showed that the major axes of a steady droplet fit the experimental ones, especially at lower capillary numbers. Chang-Zhi *et al.* [5] performed a three-dimensional (3D) numerical study. They investigated the deformation of a droplet in shear flow with unit viscosity ratio using diffuse interface method.They compared the values of deformation parameter with the results obtained by the volume of fluid (VOF) method [6], and concluded that the deformation parameter increased with the capillary number. Janssen *et al.* [7] introduced a new boundary integral method and applied it to study droplet deformation under shear flow between two parallel walls for non-unit viscosity ratio systems. For this purpose, the Green's function was modified to obey the no-slip condition at the walls. It was found that for moderate capillary numbers, the behavior of low-viscosity droplets are similar to that of droplets with unit viscosity ratio. The results also showed that for high viscosity ratio, as the confinement ratio increases the possibility of droplet rotation decreases, leading to a larger deformation and less overshoot in the droplet axes.

Inamuro *et al.* [8] presented a lattice Boltzmann method (LBM) for multi-component immiscible fluids for various values of viscosity ratios with density ratio of unity. They used the method to investigate the deformation and break-up of a droplet in shear flows with confinement ratio of 0.5. The simulation results showed that increasing the Reynolds number leads to easier deformation and break-up. Wagner *et al.* [9] used the lattice Boltzmann method to investigate the effect of inertia on the deformation and breakdown of stability of a 2D droplet surrounded by a fluid of equal viscosity in confined geometry. They showed that the increase in inertia produced larger deformation. More recently, van der Sman *et al.* [10] carried out a 2D numerical study to examine the effects of dimensionless parameters on deformation and break-up of an emulsion droplet in simple shear flow for various capillary number and viscosity ratios up to 5. It was observed that at increased viscosity ratios, the droplet deformation increases. A significant deviation from the ellipsoidal shape was seen at high capillary numbers. They also showed that the realistic physical behavior of droplet deformation could be obtained by using LBM, as long as some dimensionless numerical parameters were within certain ranges. Otherwise the droplet was either dissolved or did not deform to stable shapes at subcritical capillary numbers.

The aim of the present paper is to apply a recently proposed LBM [11, 12], which is based on the Cahn-Hilliard diffuse interface theory for binary fluids, to study droplet deformation in linear shear flow. Compared with other two-phase LBMs based on [13, 14], the present LBM is capable of eliminating the parasitic currents and dealing with higher density and viscosity ratios, but it could be more computationally expensive. The effects of viscosity ratio, capillary number, Reynolds number, and confinement ratio on droplet deformation and break-up in moderately and highly confined shear flows will

be investigated. The paper is organized as follows: In Section 2, the lattice Boltzmann method used in this paper is briefly reviewed. Section 3 presents the validation of the numerical method for a moderately confined droplet. In Section 4, the simulation of a highly confined droplet will be carried out. Section 5 provides a summary of important results obtained in this study.

2 Lattice Boltzmann method for binary fluids

Two particle distribution functions, g_α and h_α, are used in the present LBM for binary fluids [12]. The function h_α is used as a phase-field function for the transport of the composition C of one component, and the function g_α is used for the calculation of pressure and momentum of the two-component mixture. The discrete Boltzmann equations for the phase-field advection equation and the pressure evolution and momentum equations are, respectively:

$$\frac{\partial h_\alpha}{\partial t}+\mathbf{e}_\alpha\cdot\nabla h_\alpha=-\frac{h_\alpha-h_\alpha^{eq}}{\lambda}+(\mathbf{e}_\alpha-\mathbf{u})\cdot\left[\nabla C-\frac{C}{\rho c_s^2}(\nabla p-\mu\nabla C)\right]\Gamma_\alpha+\nabla\cdot(M\nabla\mu)\Gamma_\alpha, \quad (2.1)$$

$$\frac{\partial g_\alpha}{\partial t}+\mathbf{e}_\alpha\cdot\nabla g_\alpha=-\frac{g_\alpha-g_\alpha^{eq}}{\lambda}+(\mathbf{e}_\alpha-\mathbf{u})\cdot\left[\nabla\rho c_s^2(\Gamma_\alpha-\Gamma_\alpha(0))+\mu\nabla C\Gamma_\alpha\right], \quad (2.2)$$

where the equilibrium distribution functions are given as

$$h_\alpha^{eq}=t_\alpha C\left[1+\frac{\mathbf{e}_\alpha\cdot\mathbf{u}}{c_s^2}+\frac{(\mathbf{e}_\alpha\cdot\mathbf{u})^2}{2c_s^4}-\frac{\mathbf{u}\cdot\mathbf{u}}{2c_s^2}\right], \quad (2.3)$$

$$g_\alpha^{eq}=t_\alpha\left[p+\rho c_s^2\left(\frac{\mathbf{e}_\alpha\cdot\mathbf{u}}{c_s^2}+\frac{(\mathbf{e}_\alpha\cdot\mathbf{u})^2}{2c_s^4}-\frac{\mathbf{u}\cdot\mathbf{u}}{2c_s^2}\right)\right]. \quad (2.4)$$

In the above equations, $\mathbf{e}_\alpha$ is the α direction microscopic particle velocity, $\mathbf{u}$ is the volume averaged velocity, c_s is the lattice speed of sound, ρ is the mixture density, p is the dynamic pressure, λ is the relaxation time, μ is the chemical potential, t_α is the weighting factor and M is the mobility in the Cahn-Hilliard diffusion. Γ_α is defined as

$$\Gamma_\alpha=t_\alpha\left[1+(\mathbf{e}_\alpha\cdot\mathbf{u})/c_s^2+(\mathbf{e}_\alpha\cdot\mathbf{u})^2/2c_s^4-(\mathbf{u}\cdot\mathbf{u})/2c_s^2\right]. \quad (2.5)$$

The composition, momentum and dynamic pressure can be obtained by taking the moments of h_α and g_α:

$$C=\sum_\alpha h_\alpha, \quad (2.6a)$$

$$\rho\mathbf{u}=\frac{1}{c_s^2}\sum_\alpha\mathbf{e}_\alpha g_\alpha, \quad (2.6b)$$

$$p=\sum_\alpha g_\alpha. \quad (2.6c)$$

For detailed discretization of Eqs. (2.1)-(2.2) and boundary conditions, readers are referred to [12].

The mixture density ρ can be computed as $\rho=\rho_h C+\rho_l(1-C)$, where ρ_h and ρ_l are the bulk densities of two fluids. The mixing energy density for binary fluids can be written as $E_0(C,\nabla C)=E_0(C)+\kappa|\nabla C|^2/2$, where κ is the gradient parameter and $E_0(C)=\beta C^2(1-C)^2$ is the bulk energy density with constant β [15]. The equilibrium profile is obtained by minimizing the mixing energy. The equilibrium interface profile is then $C(z)=1/2+\tanh(2z/D)/2$, where z is the coordinate normal to the plane interface and D is the numerical interface thickness. Having D and interfacial tension σ, β and κ can be determined as $\beta=12\sigma/D$ and $\kappa=\beta D^2/8$.

3 2D droplet deformation in moderately confined shear flow

3.1 Validation

In this section, the deformation of an equilibrium droplet in simple shear flow generated by the motion of top and bottom walls with opposite velocities $U=\pm H\dot{\gamma}/2$ is studied, where H is the distance between the two walls, and $\dot{\gamma}$ is the shear rate. All simulations are started with an initially circular droplet placed at the center of a channel, as shown in Fig. 1. The height of the channel is four times the droplet radius following [10]. Simulations are conducted until a steady-state shape is reached.

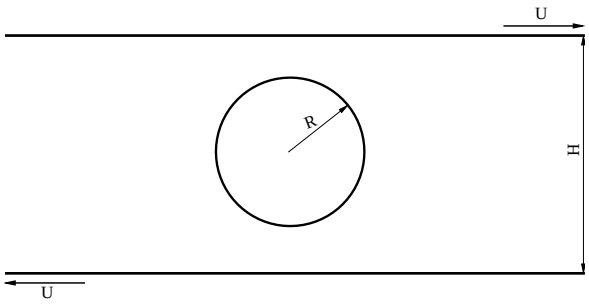

Figure 1: Schematic representation of a droplet with initial radius R in a matrix fluid located between two parallel plates with a distance between the plates of H.

The dimensionless parameters that are related to the deformation of a droplet in shear flow are the viscosity ratio $\eta=\mu_d/\mu_m$, confinement ratio $2R/H$, capillary number $Ca=\dot{\gamma}R\mu_m/\sigma$, and Reynolds number $Re=\rho\dot{\gamma}R^2/\mu_m$, where μ_d is the droplet viscosity, μ_m is the matrix viscosity, and σ is the interfacial tension. The droplet deformation is expressed by the Taylor deformation parameter,

$$D_f=\frac{a-b}{a+b}, \tag{3.1}$$

where a and b are the major and minor axes of a deformed droplet, respectively. To evaluate the Taylor deformation and the orientation angle θ, the method of moments is used (see Appendix), but this method is applicable only for low capillary number, where the droplet is nearly ellipsoidal [10].

To validate our results, first we compare the droplet deformation versus dimensionless time with the simulations performed by Sheth and Pozrikidis [16]. They used a variation of the immersed boundary formulation [17] in conjunction with a finite-difference method for solving the equations for 2D incompressible Newtonian flows. Our Lattice Boltzmann simulations were carried out for $Re=1$, $\lambda=1$, and $Ca=0.4$, and the channel has a 128×128 grid with $D2Q9$ lattice. According to Fig. 2, the result of the current study displays good agreement with that obtained by the immersed boundary formulation.

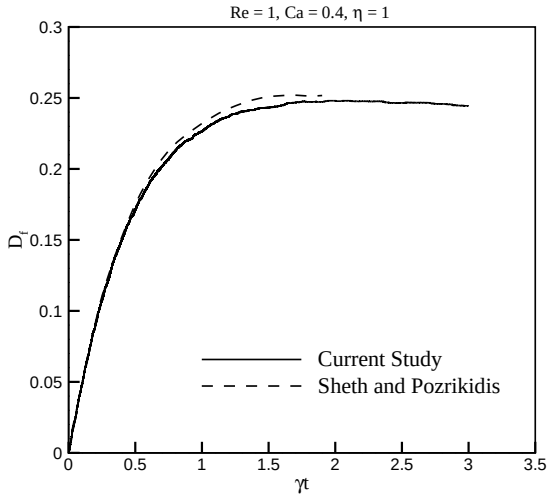

Figure 2: Comparison of droplet deformation with the result obtained by Sheth and Pozrikidis [16].

Grid dependency of the results is tested by repeating the calculations using systematically refined grids with four different grid resolutions; 64×32, 128×64, 256×128, and 512×256, corresponding to a droplet radius of 8, 16, 32, and 64, respectively. Fig. 3 shows steady state droplet shapes for these four grid sizes by contour lines for $C=0.5$. From the figure it is concluded that the result on the 128×64 grid does not exhibit any noticeable difference from the results on finer grids. Thus the channel with the grid size of 128×64 will be used in the following sections for droplet simulation subjected to shear flow.

The present LBM conserves global mass by incorporating the potential form of the intermolecular forces for binary fluids and the bounce-back rule, and also by eliminating the parasitic currents around the interface and wall regions [11, 12]. If m_0 is the initial mass of the system and m is the transient mass of the system at each time step, the ratio of m/m_0 versus the time step is shown in Fig. 4. The droplet radius, capillary number, Reynolds number, and viscosity ratio are $R=32$, $Ca=0.1$, $Re=6$, and $\eta=1$, respec-

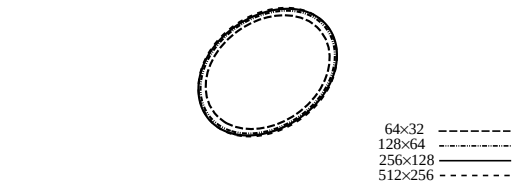

Figure 3: Droplet steady shapes depicted by contour lines of $C=0.5$ for various grid resolutions.

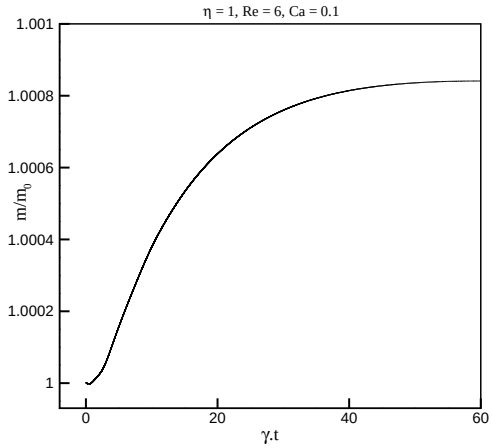

Figure 4: The time evolution of mass of the system to initial mass of the system.

tively. The computational domain has a 256×128 grid. The figure shows that m/m_0 ratio slightly increases with time, and eventually approaches a constant value, when the system reaches equilibrium.

3.2 Droplet deformation in shear flow for moderate confinement ratio

According to Janssen *et al.* [18], there exist three distinct flow regimes based on the confinement ratio $2R/H$. For $2R/H<0.3$, the effect of confinement is insignificant. The droplet is located far enough from the confining walls, and the flow field can be taken as unconfined. For $0.3<2R/H<0.5$, where the degree of confinement is moderate, the droplet is aligned more in the flow direction and the steady state droplet deformation increases with increasing confinement ratio at a given capillary number. At this confinement ratio, one cannot expect that the walls have a significant stabilizing effect on flow behavior around the droplet. Finally, for $2R/H>0.5$, the flow field is characterized by high degree of confinement. Due to the large confinement ratio in this regime, the droplet deformation and its orientation are limited by the presence of the walls.

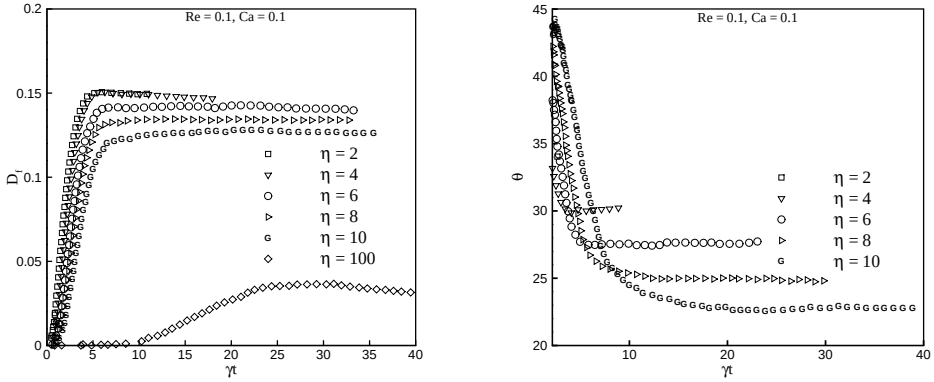

(a) Drop deformation (b) Drop orientation angle

Figure 5: (a) Deformation and (b) orientation angle of droplet versus rescaled time for $Re=0.1$, $Ca=0.1$, and various η: 2,$\cdots$,10,100.

Simulations are performed for confinement ratio of 0.5, which is at the upper limit of moderate confinement ratio. Various viscosity ratios are considered in order to investigate its effects on droplet deformation. There are several theoretical relations for drop deformation. Among them, the Taylor relation for small capillary number is given as $D_f = Ca(16+19\lambda)/(16+16\lambda)$, which shows negligible impact of the viscosity ratio. Therefore for all viscosity ratios, as long as $Ca<1$, the droplet shape will be approximately spherical [19]. Fig. 5 illustrates the deformation and orientation angle of a droplet for $\eta=2,\cdots,10,100$, $Re=0.1$, and $Ca=0.1$. As the viscosity ratio is increased, the droplet deformation decreases. As this ratio reaches 100, the final steady shapes of the droplet are not very different from its initial shape. According to Fig. 5(b), the droplet orients more in the flow direction with increasing η. Steady state droplet shapes for various viscosity ratios are shown in Fig. 6. It can be seen from the figure that although the viscosity ratio is important in determining the rate of drop deformation, the variation of drop deformation

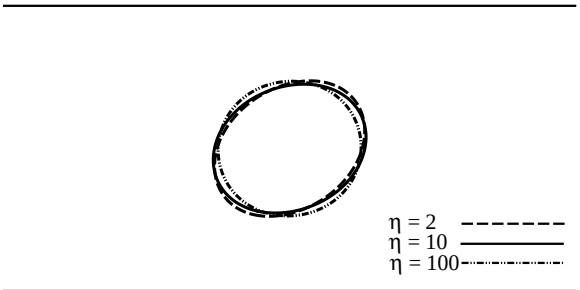

Figure 6: Contour lines of $C=0.5$ for $Re=0.1$, $Ca=0.1$, and various η: 2, 10, 100.

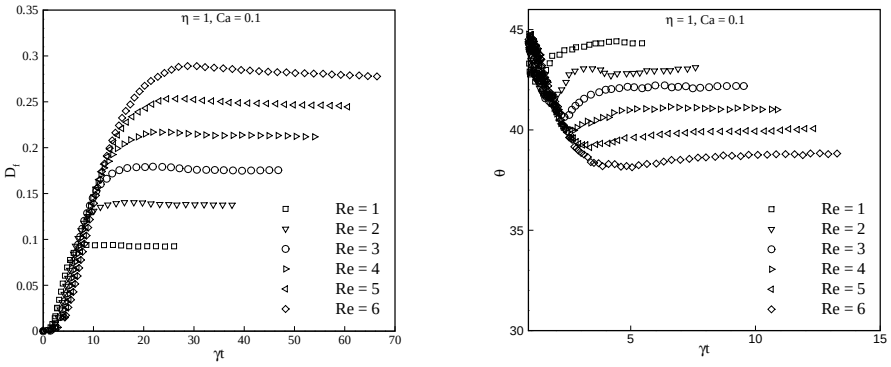

(a) Drop deformation (b) Drop orientation angle

Figure 7: (a) Deformation and (b) orientation angle of droplet versus rescaled time for $\eta=1$, $Ca=0.1$, and various Re: $1,\cdots,6$.

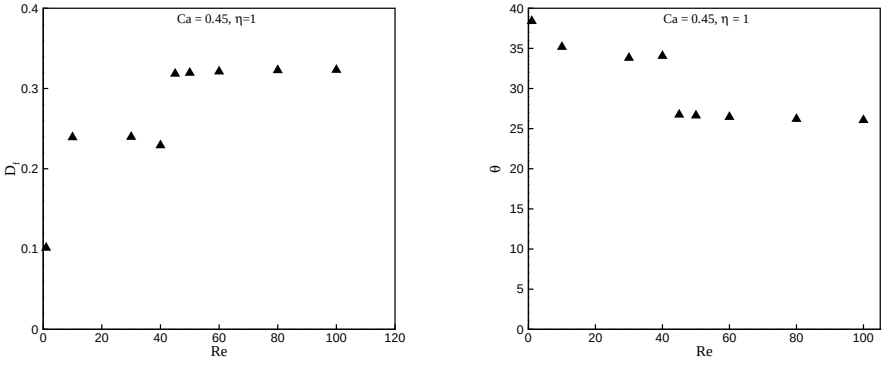

(a) Drop deformation (b) Drop orientation angle

Figure 8: (a) Deformation and (b) orientation angle of droplet versus Re around critical Ca.

is not significantly changed by increasing η.

The effect of inertia on droplet deformation in shear flow is also investigated. The simulations are performed at $Ca=0.1$ and $\eta=1$. The Reynolds number is varied in the range $1<Re<6$. Fig. 7 shows the evolution of D_f and the orientation angle θ. As the Reynolds number increases, inertial force starts to play an important role in determining the equilibrium droplet shape, and thus the droplet becomes increasingly elongated. As shown in Fig. 7(b), the droplet orients more in the flow direction with increasing Re, but the orientation angle still remains smaller than $\pi/4$ for all values of Re at $Ca=0.1$. To investigate the effect of inertia on droplet deformation near and below critical capillary number, the simulations are conducted on 128×64 grid. The initial radius of droplet has 16 lattice units. It can be seen from Fig. 8 that for large Reynolds numbers, the deforma-

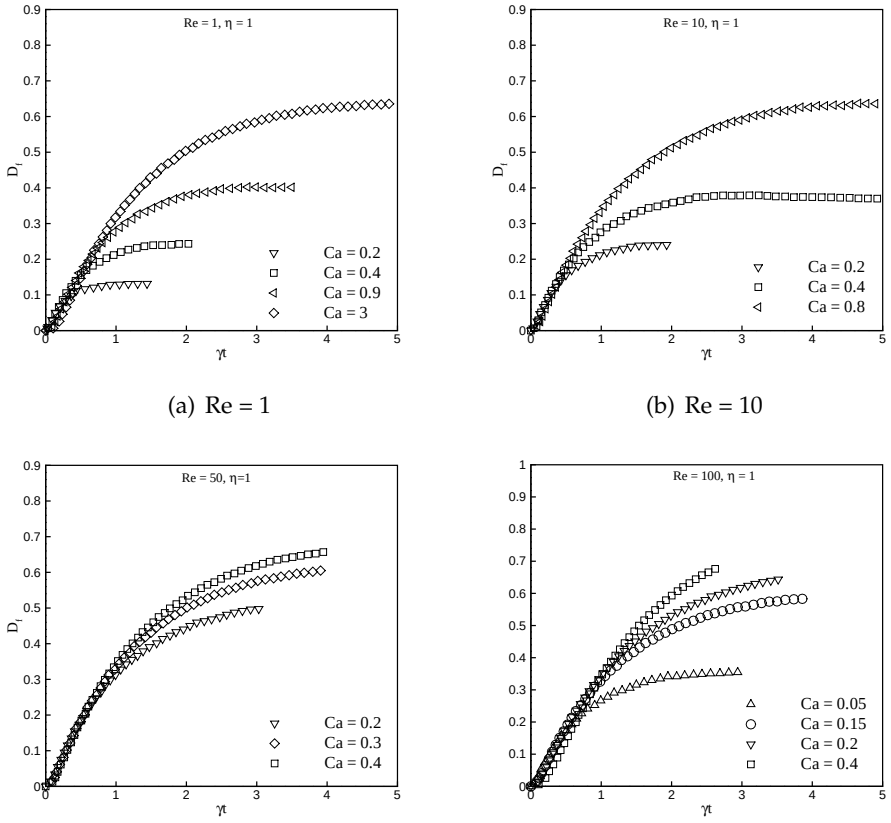

(a) Re = 1 (b) Re = 10

(c) Re = 50 (d) Re = 100

Figure 9: The evolution of droplet deformation in dimensionless time for $\eta=1$, and (a) $Re=1$, (b) $Re=10$, (c) $Re=50$, and (d) $Re=100$.

tion and orientation angle are approximately constant. This behavior of a droplet can be explained by the fact that the droplet approached the inviscid limit for large Reynolds numbers [20].

Now different combinations of viscosity ratio, Ca, and Re for a droplet with 32 lattice units are studied. We consider four different cases, whose Reynolds number ranges from zero to 100 with different values of capillary number. According to Fig. 9, for a fixed value of viscosity ratio and Reynolds number, increasing the capillary number, i.e. decreasing the interface tension, increases droplet deformation. The droplet deformation is also increased with increasing Reynolds number, while keeping all other parameters constant. In Fig. 9, for all cases there is a critical capillary number, below which the droplet deforms and obtains a stationary shape, but above which the droplet does not reach a steady shape and continues to deform and elongate under the action of the shearing flow generated by the motion of the walls. By increasing the inertia effect this critical value

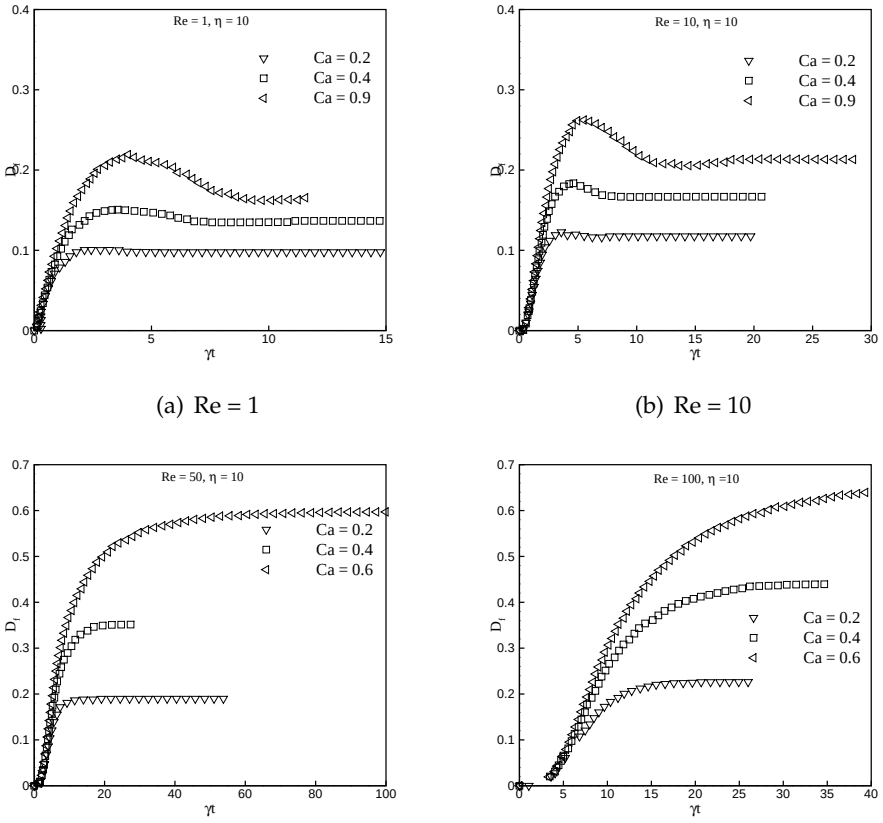

(a) Re = 1 (b) Re = 10

(c) Re = 50 (d) Re = 100

Figure 10: The evolution of droplet deformation in dimensionless time for $\eta = 10$, and (a) $Re = 1$, (b) $Re = 10$, (c) $Re = 50$, and (d) $Re = 100$.

decreases, which is in agreement with the results of Sheth and Pozrikidis [16]. For instance, the critical value of capillary number for Fig. 9(b) ($Re = 10$, $\eta = 1$) is around 0.9, while the critical capillary number for Fig. 9(d) ($Re = 100$, $\eta = 1$) is around 0.4. It should be noted that although the abrupt termination for cases with $Re = 50$ and $Re = 100$ at $Ca = 0.4$ indicates instability of the droplet, all other cases with sharp termination need longer simulation time to reach the steady state shape.

The results for relatively high values of viscosity ratio are shown in Fig. 10. By comparing the corresponding deformation curves in Figs. 9 and 10, it is concluded that the droplet deformation decreases as the viscosity ratio increases, which is an expected property of the deformation of a viscous droplet. Accordingly, the critical value of capillary number increases with increasing viscosity ratio. To show the effect of inertia on droplet deformation more clearly, interfacial shapes of droplet for different values of Reynolds number are depicted in Figs. 11(a) to 11(d), while keeping other parameters constant. In

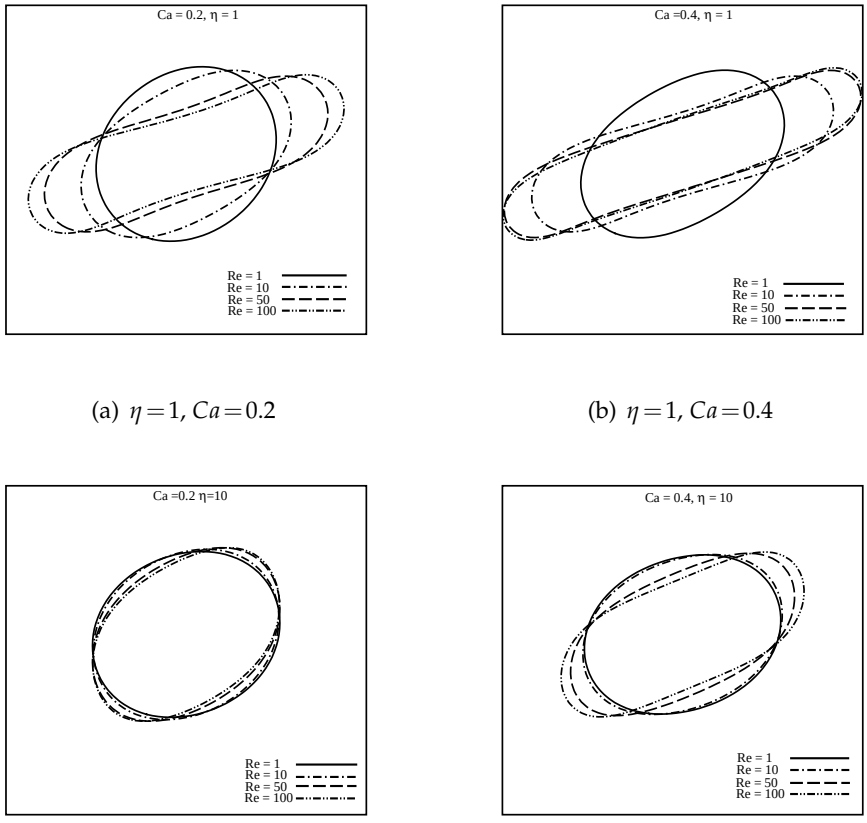

(a) $\eta=1$, $Ca=0.2$ (b) $\eta=1$, $Ca=0.4$

(c) $\eta=10$, $Ca=0.2$ (d) $\eta=10$, $Ca=0.4$

Figure 11: Steady state droplet shapes for (a) $\eta=1$ and $Ca=0.2$, (b) $\eta=1$ and $Ca=0.4$, (c) $\eta=10$ and $Ca=0.2$, and (d) $\eta=10$ and $Ca=0.4$.

each figure, the solid, dot-dashed, dashed and dot-dot-dashed lines correspond to steady state shapes for $Re=1$, $Re=10$, $Re=50$, and $Re=100$. As can be seen for $Re=50$, and $Re=100$ at $Ca=0.4$ and $\eta=1$, the droplet does not reach steady state. Therefore, for the moderately confined droplet the final steady shape of mildly deformed droplets is nearly elliptical, while highly deformed droplets have sigmoidal shapes.

To illustrate the effect of inertia on the structure of the flow inside the droplet, in Fig. 12 we present streamline patterns for three different Reynolds numbers (Re=1, 10, 50) corresponding to the shapes shown in Fig. 11(a). The figures confirm that the effect of inertia is not only on the shape of the droplets (Fig. 11(a)), but also on the structure of the flow inside and around the droplets. The reversing flow seen in the middle of the channel to either side of the droplet results from both the interaction with the walls and the inertia [21–23]. In all three cases, the droplet interfaces are tangential to the streamlines

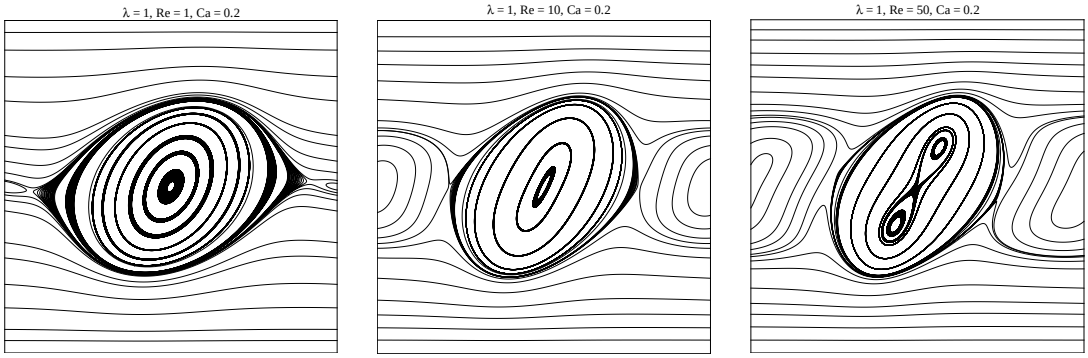

(a) $Re=1$ (b) $Re=10$ (c) $Re=50$

Figure 12: Streamline patterns of flow structure inside and around the droplet for $\eta=1$, $Ca=0.2$, and (a) $Re=1$, (b) $Re=10$, (c) $Re=50$.

meaning that the droplets have reached steady-state shapes. As the Reynolds number is increased, the inclination of streamlines inside the droplets decrease, which corresponds to the reduction of the orientation angle of droplets shown in Fig. 11(a).

3.3 Droplet break-up in moderately confined shear flow

In this section, we show break-up of a droplet in simple shear flow. The prediction of the critical conditions beyond which steady droplet shape cannot be observed has been investigated in the literature. If an initially circular droplet is placed in a shear flow, the droplet deforms, and finally reaches a stationary shape. When the capillary number exceeds a critical value, the transient elongation of droplet is started, and the droplet cannot maintain a steady shape, which ends with break-up. Although most of the break-up has a binary nature, ternary break-up can occur if the droplet length is larger than six undeformed drop radii i.e. $6R$ [18]. Depending on the confinement ratio, ternary break-up may also occur. It has been shown that there is a critical confinement ratio at which the break-up changes from binary to ternary or multiple break-ups [18]. We considered three different values of Reynolds number with their critical Ca at $\eta=1$. The critical capillary number is the lowest value of Ca at which an initially circular droplet breaks up.

Figs. 13-15 show snapshots of the break-up process for various Reynolds numbers. It is observed that as the droplet is stretched, it first becomes ellipsoidal in shape. The minor axis shrinks while the major axis lengthens, which leads to the formation of a waist near the center of the droplet. Consequently, the droplet changes from ellipsoidal shape to dumbbell shape. The bulbs at the end of the droplet achieve a stable shape and the center of the droplet becomes even thinner. Eventually a neck emerges between the central portion of the droplet and bulbs. From the figures it can be concluded that by increasing the Reynolds number, the critical value of capillary number, at which break-up occurs, decreases. Fig. 16 compares the evolution of droplet *vs.* time for two values

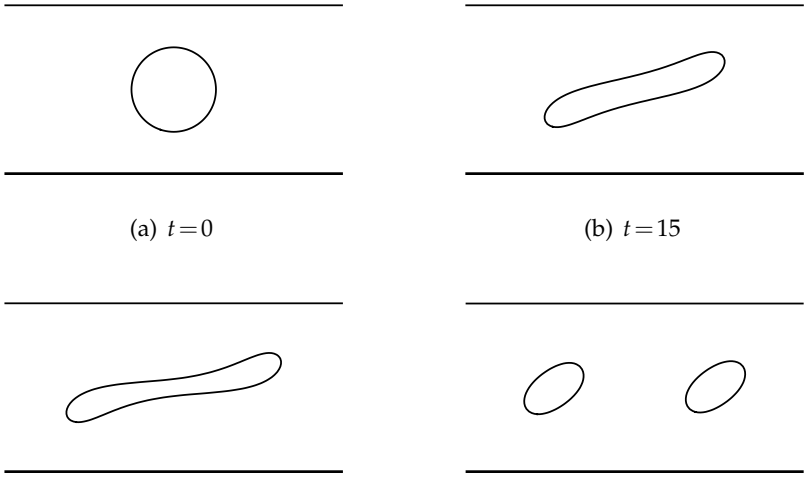

(a) $t=0$ (b) $t=15$

(c) $t=25$ (d) $t=100$

Figure 13: Snapshots of droplet break-up for $\eta=1$, $Ca_{crit}=0.8$, and $Re=2$.

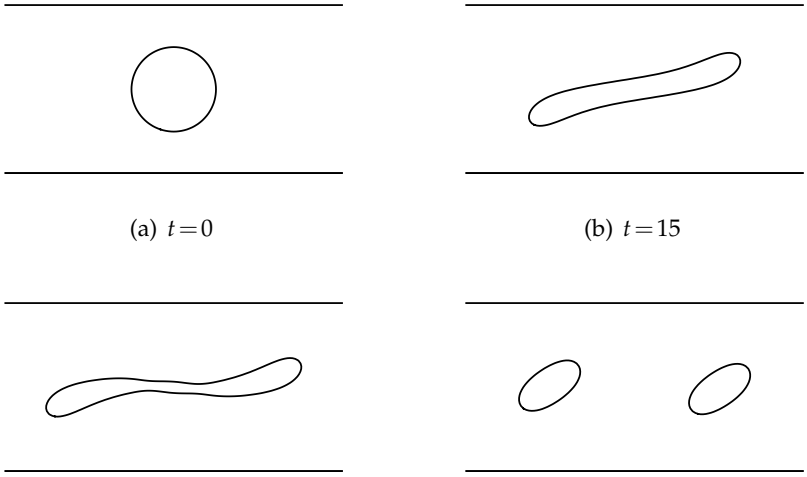

(a) $t=0$ (b) $t=15$

(c) $t=30$ (d) $t=91$

Figure 14: Snapshots of droplet break-up for $\eta=1$, $Ca_{crit}=0.2$, and $Re=10$.

of Reynolds number. The droplet at $Re=10$ has an overshoot that takes the droplet to significant enough deformation that it breaks at $t=21.7$. The case with $Re=2$ has an overshoot that is not high enough to cause break-up.

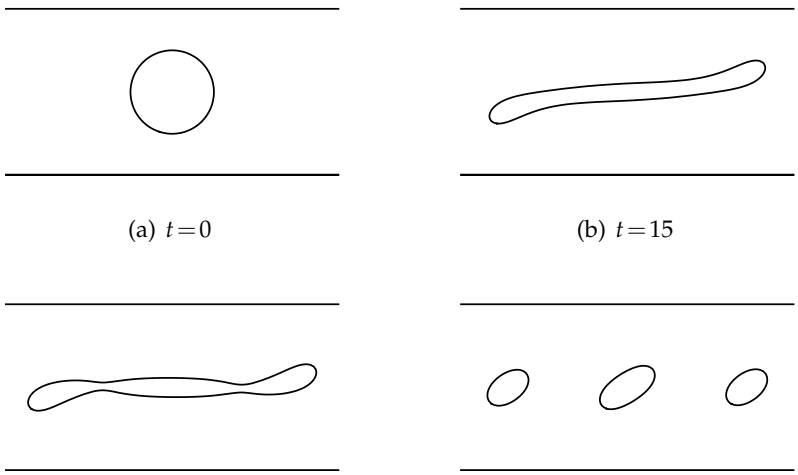

(a) $t=0$ (b) $t=15$

(c) $t=20$ (d) $t=83$

Figure 15: Snapshots of droplet break-up for $\eta=1$, $Ca_{crit}=0.03$, and $Re=100$.

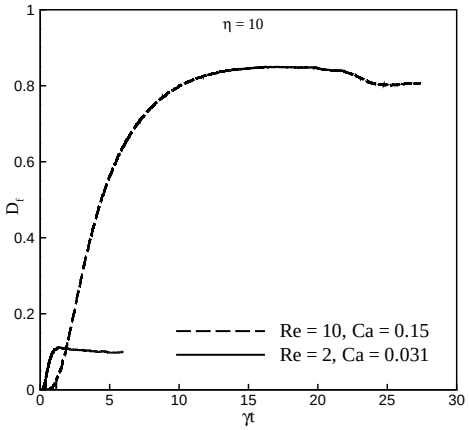

Figure 16: Droplet evolution versus time for 2D droplet.

4 Droplet deformation in highly confined shear flow in 3D

Most of the literature on shear flow-induced droplet deformation is devoted to the flow in an unconfined situation, in which the droplet is located far from the confining walls. If this condition is not satisfied, wall effects are expected to influence the flow behavior of a nearby droplet. Therefore, droplet-wall interactions could play an important role and affect the dynamics of droplet deformation. In this section, an investigation of the effects of viscosity ratio and degree of confinement on the dynamics of a single 3D droplet has been

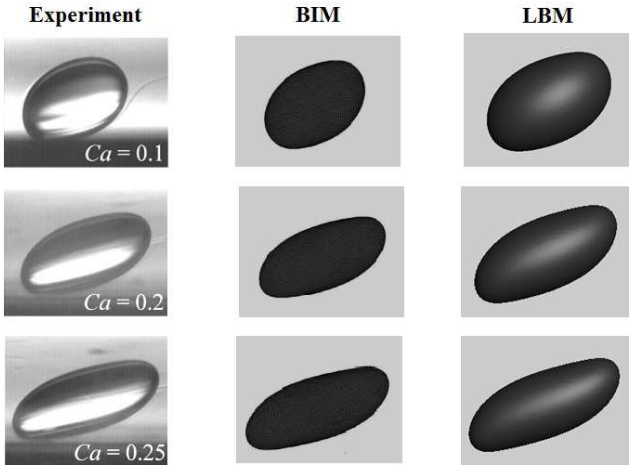

Figure 17: Steady state droplet shapes at $Ca=0.1$, 0.2, and 0.25 (from top to bottom) for $2R/H=0.8$.

performed. The steady state shapes of a confined droplet with a degree of confinement of $2R/H=0.8$ at different capillary numbers are shown in Fig. 17. The computational domain is divided into a $200\times62\times100$ cubic $D3Q27$ lattice. In the first column, the experimentally observed shapes are recorded in the velocity-velocity gradient plane [24] are depicted. The corresponding shapes calculated from BIM and LBM are shown in the second and third columns, respectively. A good agreement between the results of LBM, BIM and experimental images is found for all three capillary numbers. The images show a decrease in orientation angle and thus more orientation toward the flow direction, with increasing capillary number. Fig. 18 shows the dimensionless axes ($L/2R$, and $B/2R$)

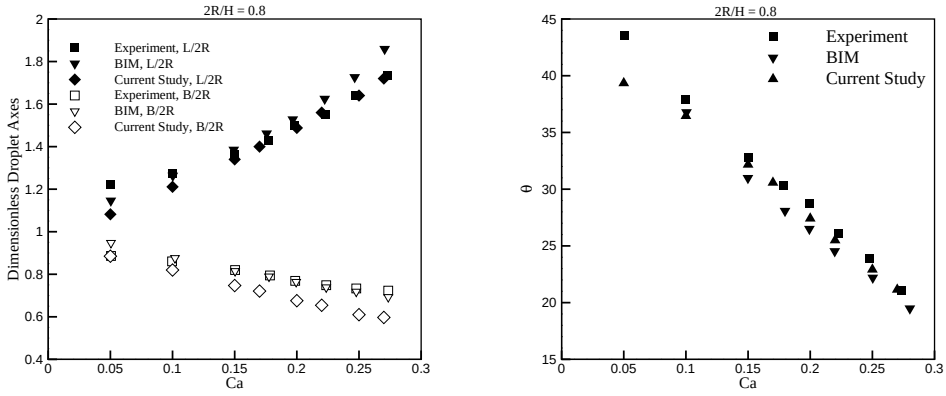

(a) Drop deformation (b) Drop orientation angle

Figure 18: Comparison between experimental data and numerical simulations for $2R/H=0.8$ as a function of capillary number: (a) Dimensionless droplet axes and (b) orientation angle.

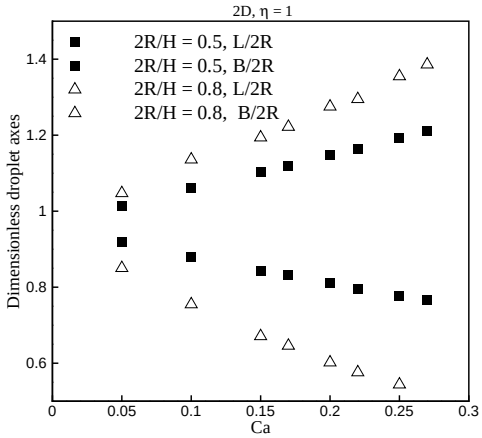

Figure 19: Effect of confinement ratio on droplet deformation as a function of Ca.

and the orientation angle as a function of Ca for a highly confined droplet. It is clear that confinement affects the deformation of a droplet at a given Ca. In Fig. 19, the steady state deformation of a droplet is shown for two confinement ratios as a function of Ca for a viscosity ratio of 1. The droplet with $2R/H=0.5$ is only weakly confined whereas the droplet with $2R/H=0.8$ has a relatively high degree of confinement. In a highly confined channel, not only the magnitude of the deformation, but also the shape of the deformed droplet is changed due to the proximity of the walls. Instead of an ellipsoid, which is the characteristic shape for droplets in a bulk shear flow, a sigmoidal deformation is present in a confined shear flow. Fig. 20 shows the deformation of confined droplets for two

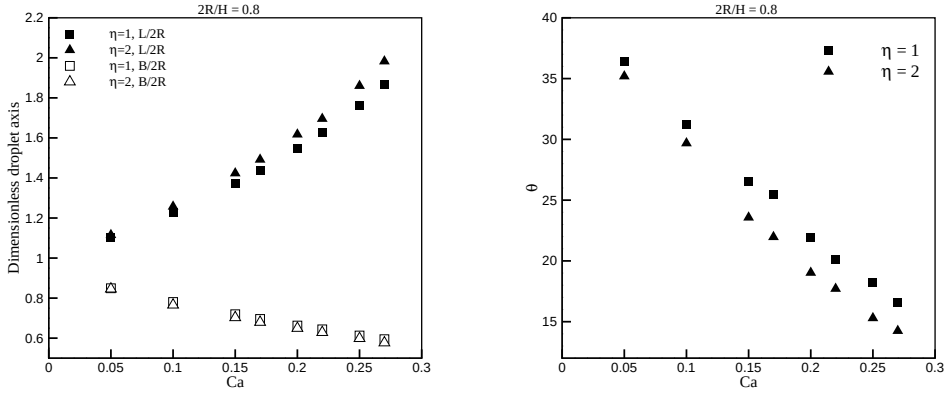

(a) Drop deformation (b) Drop orientation angle

Figure 20: (a) Dimensionless droplet axes and (b) orientation angle of confined droplets for two viscosity ratios as a function of Ca.

viscosity ratios as a function of Ca. The square symbols represent the major and minor dimensionless axes and the orientation angle of droplet for the viscosity ratio of $\eta=1$, and the triangle symbols are the results for the viscosity ratio of $\eta=2$. From Fig. 20(a) it can be seen that droplet deformation increases when viscosity ratio increases, but in turn the droplet orients more in the flow direction. On the other hand, drops with high-viscosity are hindered from rotating in shear flow, which results in a larger deformation.

5 Summary

Droplet deformation and break-up in confined shear flow were investigated by changing viscosity ratio, Reynolds number and capillary number using the lattice Boltzmann method (LBM) based on the Cahn-Hilliard diffuse interface approach. To describe confined droplets the effect of the confinement ratio was taken into account. As the viscosity ratio is increased, the droplet deformation decreases and the droplet orients more in the flow direction. It was also concluded that the variation of drop deformation is not significantly affected by increasing η. To illustrate the effect of inertia in determining the equilibrium droplet shape, the effect of Reynolds number was investigated. By increasing Re, the droplet becomes increasingly elongated and aligns more toward the flow direction. It was also shown that for large Reynolds numbers, the deformation and orientation angle of a moderately confined droplet near critical capillary number are approximately constant, which is in agreement with the 3D results obtained by Renardy [20]. The dependency of the critical capillary number, above which the final steady state shape of a droplet cannot be found and break-up may possibly occur, on the viscosity and inertia was shown. It was concluded that by increasing the Reynolds number, the critical value of capillary number decreases. Increasing the confinement ratio leads to enhanced deformation that results in a non-ellipsoidal (sigmoidal) droplet shape. These effects are more pronounced at high Ca. In highly confined channels, droplets are prevented from rotating in shear flow by increasing the viscosity ratio, which leads to a further deformation.

Appendix: Method of moments

Since the order parameter in this simulation is composition C, the moments are the following

$$M_0 = \iint C dx dx, \tag{A.1a}$$

$$M_{1\alpha} = \frac{1}{M_0} \iint C x_\alpha dx dx, \tag{A.1b}$$

$$M_{2\alpha\beta} = \iint C\left(x_\alpha - \bar{x}_\alpha\right)\left(x_\beta - \bar{x}_\beta\right) dx dx, \tag{A.1c}$$

where x_α and x_β are the grid points and $\bar{x}_\alpha$ and $\bar{x}_\beta$ are the centers of gravity, which are equal to the second moment of inertia. It should be noted that the order parameter is

equal to C if it is positive and is zero if it is negative. In the cases that the droplet takes the ellipsoidal shape and has an orientation angle of θ the Mohr circle scheme is used to compute a, b and θ.

$$a = 2\sqrt{D_1}, \tag{A.2a}$$

$$b = 2\sqrt{D_2}, \tag{A.2b}$$

$$\theta = \frac{1}{2}\arctan\left(\frac{2M_{2xy}}{M_{2yy}-M_{2xx}}\right), \tag{A.2c}$$

where

$$D_1 = \frac{\left(M_{2yy}(\cos\theta)^2 - M_{2xx}(\sin\theta)^2\right)}{\cos(2\theta)}, \tag{A.3a}$$

$$D_2 = \frac{\left(M_{2xx}(\cos\theta)^2 - M_{2yy}(\sin\theta)^2\right)}{\cos(2\theta)}. \tag{A.3b}$$

Acknowledgments

This work was supported by the National Science Foundation PREM grant DMR-0934206.

References

[1] G.I. Taylor, Proc. Roy. Soc. 26, 501-523 (1934).
[2] R. de Bruijn, Ph.D. thesis, Eindhoven University of Technology (1989).
[3] H.P. Grace, Chem. Eng. Comm. 14, 225-277 (1982).
[4] D. Megias-Alguacil, K. Feigl, M. Dressler, P. Fischer, and E.J. Windhab, J. Non-Newtonian Fluid Mech. 126, 153-161 (2005).
[5] L. Chang-Zhi and G. Lie-Jin, Heat Transfer-Asian Res. 36, 286-294 (2007).
[6] J. Li, Y.Y. Renardy, Phys Fluids. 12, 269-282 (2000).
[7] P.J.A. Janssen and P.D. Anderson, J. Comput. Phys. 227, 8807-8819 (2008).
[8] T. Inamuro, R. Tomita, and F. Ogino, Int. J. Mod. Phys. B 17, 21-26 (2003).
[9] A.J. Wagner, L.M. Wilson, and M.E. Cates, Phys. Rev. E 68, 045301(R) (2003).
[10] R.G.M. van der Sman and S. van der Graaf, Comp. Phys. Comm. 178, 492-504 (2008).
[11] T. Lee, Comput. Math. Appl. 58, 987-994 (2009).
[12] T. Lee and L. Liu, J. Comput. Phys. 229, 8045-8063 (2010).
[13] X. Shan and H. Chen, Phys. Rev. E 47, 1815-1819 (1993).
[14] M.R. Swift, W.R. Osborn, and J.M. Yeomans, Phys. Rev. E 54, 5041-5052 (1996).
[15] D. Ertas and M. Kardar, J. Comput. Phys. 155, 96-127 (1999).
[16] K.S. Sheth and C. Pozrikidis, Comput. Fluids 24, 101-119 (1995).
[17] C.S. Peskin, J. Comp. Phys. 25, 220-252 (1977).
[18] P.J.A. Janssen, A. Vananroye, P. Van PuyveldeJ, P. Moldenaers, and P.D. Anderson, J. Rheol. 54, 1047-1060 (2010).
[19] H.A. Stone, Annu. Rev. Fluid Mech. 26, 65-102 (1994).

[20] Y.Y. Renardy, Phys. Fluids 13, 7-13 (2001).
[21] D.R. Mikulencak and J.F. Morris, J. Fluid Mech. 520, 215-242 (2004).
[22] M. Zurita-gotor, J. Blawzdziewicz, and E. Wajnryb, J. Fluid Mech. 592, 447-469 (2007).
[23] R.K. Singh and K. Sarkar, J. Fluid Mech. 683, 149-171 (2011).
[24] A. Vananroye, P.J.A. Janssen, P.D. Anderson, P. Van PuyveldeJ, and P. Moldenaers, Phys. Fluids 20, 013101 (2008).